Cytoplasmic strains and strain rates in motile polymorphonuclear leukocytes

Scott I. Simon and Geert W. Schmid-Schönbein
Department of AMES-Bioengineering, University of California, San Diego, La Jolla, California 92093 USA

ABSTRACT A new method is presented to measure local cytoplasmic deformation and rate of deformation in motile active neutrophils. The deformation is expressed in terms of biomechanical strains and strain rates. For this purpose small phagocytosed latex microspheres were used as intracellular markers. Planar Lagrangian and Eulerian strains and the rate of strain were estimated from the positions of a triad of internalized markers. Principal strains, stretch ratios, and principal directions were computed. The intracellular strains were found to be large relative to the overall cell shape change. Principal cytoplasmic stretch ratios showed large extension in the direction of pseudopod formation and cell locomotion and contraction in perpendicular directions. Regional strain analysis showed contractile strains to predominate in the vicinity of the pseudopod or leading edge of motion. The transitional region between the pseudopod and the main cell body exhibited large shear strains. The posterior region, where the uropod is located, also revealed large extensions but small contractile strains. The rate of strains are relatively small, nonuniform in time, and largely independent of the strain. The method we propose to measure cytoplasmic strain can be applied to a variety of problems in cell mechanics.

INTRODUCTION

Neutrophils, like other leukocytes or connective tissue cells, can undergo spontaneous cellular motility by utilization of metabolic energy. Spontaneous motion is exhibited in a wide range of cell activities, from simple pseudopod projection to phagocytosis, transendothelial migration, or chemotaxis. The key element that drives cell motion and deforms the cytoplasm is the active motion of the cytomatrix. In response to receptor binding of chemotactic stimuli, neutrophils become hyperadhesive to the endothelium, they form pseudopods and undergo gross cell deformation, enabling the cell to migrate across the endothelium and into the tissue.

Inherent in virtually every aspect of neutrophil function is the active deformation of the cytoplasm. Intracellcular motility is frequently manifest in the form of cytoplasmic streaming. Numerous studies have attempted to unravel the mechanism of motility at the cytoskeletal level. The structural and biochemical basis of contractile events has been explored utilizing light microscopic (Allen, 1981), ultrastructural (Malech et al., 1977), and biochemical techniques (Stossel et al., 1976). Such studies have shown the cytomatrix to consist of macromobules, globular and filamentous actin, and larger organelles all distributed nonuniformly in an aqueous solution. The contractile proteins constitute a motile microfilament system which has been associated with pseudopods and ingested particles (Valerius et al., 1981). Microtubules radiating from centrioles have been shown to be associated with phagolysosomes and other granules (Berlin et al., 1978).

Changes in cell shape and cytoskeletal organization is induced by chemotactic stimuli. For example, in response to the tetrapeptide F-Met-Leu-Phe (FMLP), neutrophils develop a broad anterior lamellipodia supported by a dense meshwork of microfilaments (Davis et al., 1982). Actin is the most abundant protein in leukocytes (Allen et al., 1981; Senda et al., 1969). Proteins that have been found to interact with actin are myosin, actin-binding protein (Stossel et al., 1976), and regulatory and binding proteins, such as gelsolin, calmodulin, and filamin (Schliwa, 1986). These proteins regulate filament growth, length, and polarity. Myosin serves as the energy-transducing protein and appears to be present in the cytosol of neutrophils with enzymatic and mechanical activity (Fujiwara et al., 1976).

In contrast to straited muscle cells with stationary myofibrils which allow undirectional shortening and generation of large forces, neutrophils have a force-generating filament system of transient structures which assemble and disassemble. An example is pseudopod formation, during which the actin network forms locally by a polymerization of gelation process (Taylor and Condeelis, 1979). Neutrophils can locomote along a chemical gradient by a coordinated sequence of deformations (Zigmond, 1978) and can form constriction rings even in uniform chemotactic concentrations (Shields and Haston, 1985;

Dr. S. I. Simon's current address is Department of Immunology (IMM12), Scripps Clinic and Research Foundation, 10666 North Torrey Pines Road, La Jolla, CA 92037.

Schmid-Schönbein et al., 1982). The fine-tune control of gross cell motion is dependent upon an integrated mechanism for localized coordination of the gelation process. Although knowledge of the constituents and to a lesser extent the organization of components involved in the generation of motive force has been elucidated, details of the mechanism by which the cytoskeletal network achieves cell orientation, locomotion, or merely pseudopod projection are largely unknown. In the past, optical microscope observations have provided qualitative indices of intracellular movement or catalogues of net cell motion, but few studies have addressed the intracellular motion. In part the cytoplasmic motion is made visible by the shuttling of granules, mitochondria, and other organelles. But often these organelles are too numerous and do not lend themselves easily to continuous observation. In contrast, neutrophils with internalized microspheres offer an experimental model with which cytoplasmic motion can be studied.

It is the objective of this report to present a method to quantitatively describe the complex intracellular deformations within neutrophils in the active state. Local cytoplasmic measures of strain and strain rate are presented and a method is described to derive these quantities from the displacement history of intracellular microspheres. These tools are then applied to probe the local cytoplasmic deformation in a few selected neutrophil activities.

ANALYSIS

Marker configuration

Internalized latex microspheres which are tightly covered with plasma membrane (Simon and Schmid-Schönbein, 1988) serve as intracellular markers of cytoplasmic position. Three markers enclosing a small parcel of cell cytoplasm are used for the strain and strain rate computations. Each traid must meet the following requirements: (*a*) The three markers are not constrained in their motion by attachment to each other or to the membrane. (*b*) The distance between any pair of markers is no more than ~2.0 μm. (*c*) During the entire period of observation, the triad or at least the centroid of each marker, remains in the plane of focus.

A continuous video record of a triad of particles and the cell's contour in the focal plane were recorded at preselected time intervals. The marker coordinates were recorded relative to a fixed laboratory coordinate system. In general, the cell body experiences nonhomogeneous deformations during locomotion or local pseudopod formation. Therefore, it is necessary to confine the strain analysis to small portions of the cytoplasm with a homogeneous displacement field.

Lagrangian and Eulerian strain

To define strain, we need to select a reference shape. For example, a reproducible reference state at time $t = 0$ may be selected at the beginning of a pseudopod projection or at the beginning of a locomotory cycle. None of these reference shapes are necessarily stress free.

The position of a microsphere marker in the triad in the initial configuration is designated by a_1, a_2, a_3. The same marker has the coordinates x_1, x_2, x_3 after cytoplasmic deformation at a later time ($t > 0$) (Fig. 1). The deformation is defined by the continuous functions $x_i = x_i(a_1, a_2, a_3, t)$ for each of the three markers.

For consistency, marker No. 1 on the video record was denoted as that in the quadrant between 9:00 and 12:00, and markers No. 2 and 3 were numbered counterclockwise starting from marker No. 1 (see e.g., Fig. 3). The origin of the local triad coordinate axes is positioned at marker No. 2 and the axes are kept parallel and normal, respectively, to the television scanning line. A description of the change in distance between the three intermarker distance vectors before (ds_o at $t = 0$), and after deformation (ds at $t > 0$) serves for computation of strain (Fig. 1). Using the notation of Fung (1969), the square of the distance between two markers are given by:

$$ds_o^2 = da_1^2 + da_2^2 + da_3^2 \quad \text{(before deformation)} \qquad (1a)$$

$$ds^2 = dx_1^2 + dx_2^2 + dx_3^2 \quad \text{(after deformation).} \qquad (1b)$$

The change of distance between any two markers is given by

$$ds^2 - ds_o^2 = dx_i\,dx_i - da_j\,da_j, \qquad (2)$$

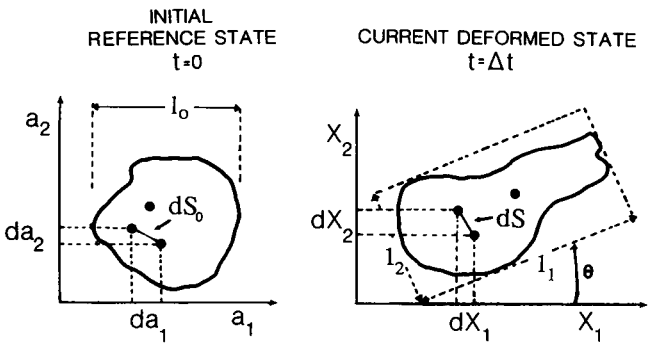

FIGURE 1 Schematic of neutrophil before and after deformation. The cell contour and three cytoplasmic markers are shown. (dS_o) Distance between two markers in the initial state with components da_1 and da_2; (dS) Distance between two markers in the current state with components dx_1, dx_2. ℓ_0 is the diameter of the cell in the initial state, ℓ_1 is the longest cell dimension during deformation, ℓ_2 is the cell dimension normal to ℓ_1. Θ is a measure for the direction of pseudopod projection.

using Einstein's summation convention for repeated indices. The Lagrangian strain may be expressed as a function of the initial reference configuration as

$$ds^2 - ds_o^2 = 2E_{ij}\, da_i\, da_j. \tag{3}$$

The Eulerian strain tensor may be expressed relative to the deformed configuration as

$$ds^2 - ds_o^2 = 2e_{ij}\, dx_i\, dx_j. \tag{4}$$

The Langrangian and Eulerian strains are:

$$E_{ij} = \frac{1}{2}\left(\delta_{\alpha\beta}\frac{\partial x_\alpha}{\partial a_i}\frac{\partial x_\beta}{\partial a_j} - \delta_{ij}\right) \tag{5a}$$

and

$$e_{ij} = \frac{1}{2}\left(\delta_{ij} - \delta_{\alpha\beta}\frac{\partial a_\alpha}{\partial x_i}\frac{\partial a_\beta}{\partial x_j}\right), \tag{5b}$$

or in terms of the displacement $u_i = x_i - a_i$

$$E_{ij} = \frac{1}{2}\left(\frac{\partial u_i}{\partial a_j} + \frac{\partial u_j}{\partial a_i} + \frac{\partial u_k}{\partial a_i}\frac{\partial u_k}{\partial a_j}\right) \tag{6a}$$

$$e_{ij} = \frac{1}{2}\left(\frac{\partial u_i}{\partial x_j} + \frac{\partial u_j}{\partial x_i} - \frac{\partial u_k}{\partial x_i}\frac{\partial u_k}{\partial x_j}\right), \tag{6b}$$

where δ_{ij} is the Kronecker symbol.

Finite strain approximation

For measurement of cytoplasmic strain, the markers are located a small but finite distance apart and remain in the plane of focus. Therefore, the computation of strain will be limited to finite plane strain. We then approximate $ds_0 = \Delta s_o$ and $ds = \Delta s$ so that Eq. 3 and 4 become:

$$\Delta s^2 - \Delta s_o^2 = 2E_{ij}\, \Delta a_i\, \Delta a_j \tag{7}$$

and

$$\Delta s^2 - \Delta s_o^2 = 2e_{ij}\, \Delta x_i\, \Delta x_j. \tag{8}$$

For a plane strain problem, three such equations are sufficient and necessary to solve for the three strain components E_{11}, E_{22}, E_{12}, or e_{11}, e_{22}, and e_{12}. Eq. 7 and 8 may be expressed as a linear algebraic problem and solved for E_{ij} in the form:

$$\begin{bmatrix} (2\,\Delta a_1^2)_1 & (4\,\Delta a_1\,\Delta a_2)_1 & (2\,\Delta a_2^2)_1 \\ (2\,\Delta a_1^2)_2 & (4\,\Delta a_1\,\Delta a_2)_2 & (2\,\Delta a_2^2)_2 \\ (2\,\Delta a_1^2)_3 & (4\,\Delta a_1\,\Delta a_2)_3 & (2\,\Delta a_2^2)_3 \end{bmatrix} \cdot \begin{pmatrix} E_{11} \\ E_{12} \\ E_{22} \end{pmatrix} = \begin{pmatrix} (\Delta s^2 - \Delta s_o^2)_1 \\ (\Delta s^2 - \Delta s_o^2)_2 \\ (\Delta s^2 - \Delta s_o^2)_3 \end{pmatrix} \tag{9}$$

where the subscript after the brackets, $(\ )_i$, i = 1, 2, 3, refers to a pair of markers in the traid, i.e., $(\ )_1$ the line element between Marker 1 and 2, $(\ )_2$ between marker 2 and 3, and $(\ )_3$ between 3 and 1.

Because the Langrangian strain tensor, E_{ij} (defined with respect to material coordinates), is symmetric, two principal strain components E_k (k = 1, 2) exist with associated principal directions $v_1^{(k)}$, $v_2^{(k)}$ (Fung, 1969). They may be computed from the eigenvalue problem:

$$(E_{ij} - E_k\,\delta_{ij})\, v_i^{(k)} = 0 \quad \text{for k} = 1, 2. \tag{10}$$

The Eulerian principal strains, e_1, e_2 are computed in a similar fashion. In the following the principle directions to be displayed are derived from the solution of the Eulerian strain eigenvalue problem.

Cytoplasmic stretch ratios

In principal coordinates, the cytoplasmic stretch ratios λ_i may be computed from the principal Lagrangian or Eulerian strains as

$$E_i = \tfrac{1}{2}(\lambda_i^2 - 1), \tag{11}$$

$$e_i = \tfrac{1}{2}(1 - 1/\lambda_i^2). \tag{12}$$

In a homogeneous deformation, the ratio of the lengths is independent of the choice for the original length ds_o. The stretch ratios represent the maximum and minimum change of length of a unit vector in the prinicipal direction. This parameter is depicted in Results in the form of line elements at the centroid of the cytoplasmic triad of markers.

Global cell stretch ratios

There is an interest to compare local cytoplasmic strains with the overall cell shape changes. We will therefore define a whole cell stretch ratio for finite deformation of the cell as measured in the same focal plane as the traid. The initial diameter of spherical cells, or the maximum length and width of undeformed cells, serve as the initial distance vectors (ℓ_o). The maximum length and the minimum width, adjacent to the traid, are the deformed distance vectors (ℓ_i) (Fig. 1). The associated stretch ratios are then computed as

$$(\lambda_{cell})_i = \frac{\ell_i}{\ell_o} \qquad \text{for i} = 1, 2. \tag{13}$$

The direction of cell elongation may be defined relative to a set of coordinates orthogonal to that of the laboratory reference. The direction of deformation is defined as the angle between the maximum distance vector and the horizontal axis as shown in Fig. 1.

Rate of deformation

In many cases the active cytoplasmic deformation resembles a continuous motion. It is therefore useful to study

cytoplasmic strain rates. The difference in velocity dv_i between two neighboring microspheres in the cytoplasm is given as

$$dv_i = \frac{\partial v_i}{\partial x_j} dx_j.$$

This can be expanded (Fung, 1969) as

$$dv_i = D_{ij}\, dx_j - \omega_{ij}\, dx_j.$$

ω_{ij} is the rate of rotation tensor which represents a rotation of the triad and is at the moment of no further physical interest, and D_{ij} is the rate of deformation tensor defined by

$$D_{ij} = \frac{1}{2}\left(\frac{\partial v_i}{\partial x_j} + \frac{\partial v_j}{\partial x_i}\right). \quad (14)$$

D_{ij} represents a measure of the instantaneous rate of change of the squared length of the distance vector (ds) between two neighboring points in the cytoplasm:

$$(ds)^2 = dx_i\, dx_i$$

and thus

$$\frac{d}{dt}[(ds)^2] = 2\, dx_i \frac{d}{dt}(dx_i). \quad (15)$$

The last term may be written in terms of the differential velocity vector (Simon, 1988)

$$\frac{d}{dt}[(ds)^2] = dx_i \left(\frac{\partial v_i}{\partial x_j} + \frac{\partial v_j}{\partial x_i}\right) dx_j \quad (16)$$

or

$$\frac{d}{dt}[(ds)^2] = \frac{1}{2}\, dx_i\, D_{ij}\, dx_j. \quad (17)$$

The rate of change of the squared length of a line element between time t (Δs^2) and time $t + \Delta t$ (ΔS^2) may be expressed in finite approximation as

$$\frac{d}{dt}[(ds)^2] = \lim_{\Delta t \to 0} \frac{\Delta s^2(t) - \Delta S^2(t - \Delta t)}{\Delta t}. \quad (18)$$

Combining Eq. 17 and 18 we can compute D_{ij} from the relationship

$$\frac{\Delta s^2 - \Delta S^2}{\Delta t} = 2\, D_{ij}\, \Delta x_i\, \Delta x_j. \quad (19)$$

Three equations for the three intermarker distances serve to compute the three components D_{11}, D_{22}, and D_{12} analogous to the computation of strain (Eq. 9). Because D_{ij} is a symmetric second-order tensor, it has two principal values and two associated principal directions. The principal values of D_{ij} represent the maximum and minimum extension rates for line elements in the principal directions.

Measurement of plane strain in neutrophils

Although plane strain is used to quantify the deformation in the cell cytoplasm, cells are three-dimensional objects with strains in all directions. The assumption of plane strain is only approximately satisfied by confining our analysis to markers which remain in the focal plane.

How then do the plane strains compare with three-dimensional strains? For a hypothetical deformation of pure or simple shear occurring in the plane of focus, as well as any plane parallel to it, there is no difference between the strains computed in the three-dimensional (E_{11}^{3d}, E_{12}^{3d}, E_{22}^{3d}) and the two-dimensional case (E_{11}^{2d}, E_{12}^{2d}, E_{13}^{2d}) (Simon, 1988).

Because the molecular organization of the cytoskeleton may lead to anisotropic material properties, a more complex hypothetical displacement field with a combination of shear in two different planes was considered. To obtain an estimate of the error due to out-of-plane shear strain, we assume that the magnitude of the shear out of the focal plane is equal to that in the plane. The largest shear for a triad of 1.0-μm-diam microspheres yielded a 72° change in the angle between two line elements orthogonal in the reference state, resulting in a final angle of 18°. Computation of the error in the strain for simple shear out of plane yields a 31% error between E_{11}^{2d} and E_{11}^{3d}. A more realistic measure for the average in-plane shear experienced by the triads in the focal plane was a 10° change from an orthogonal reference. This yields a 1% error between E_{ij}^{2d} and E_{ij}^{3s} assuming out-of-plane shear.

Microsphere displacements in which one microsphere crosses the line of the other two in the triad, leads to undefined strains. This class of nonhomogeneous deformation histories may occur within the cell, however, such cases were the exception and were not included in this analysis.

METHODS AND MATERIALS

Cell separation and microsphere phagocytosis

Human neutrophils from normal, healthy volunteers were obtained by venous puncture, collected in heparinated vacutainers and sedimented at 1 *g* in a 37°C water bath. The media used for cell incubation was Hanks (Gibco, Grand Island, NY) buffered with HCO_3 to a pH of 7.45, and 20% homologous plasma. Three sizes of polystyrene latex microspheres (Dow Corning Corp., Midland, MI) were used for cell phagocytosis: 0.6, 1.0, and 2.0 μm in diameter. The microspheres were opsonized to

achieve phagocytosis using the same protocol as described previously (Simon and Schmid-Schönbein, 1988).

An observation chamber was designed for the study of freshly-drawn cell suspensions. Cells are placed in this chamber and viewed through a high-resolution inverted light microscope (E. Leitz, Inc., Wetzlar, FRG).

The cell/microsphere suspension (25 μl) with $\sim 10^3$ cells was mixed with 0.75 ml buffer and placed into the observation chamber at 37°C. Single cells which lightly adhered to the cover glass were viewed in various states of particle engulfment, but the analysis was performed on cells which had only a few internalized microspheres and had maintained an excess of plasma membrane during cytoplasmic motile activity.

Micropipette aspiration and stimulus application

A selected set of cells was stimulated with the chemotactic substance FMLP (10^{-7} M), treated with cytochalasin D (0.5 μg/ml) or EDTA (1 g%) as required. These substances were applied through a micropipette either locally on to single cells, or to a region with several cells. In this way several different neutrophil responses could be elicited: chemotaxis by local FMLP stimulation, or chemokinesis by subjecting the cells to a more uniform concentration of FMLP. Spontaneous chemokinesis possibly due to cytokine release was also observed in control populations without FMLP infusion. The same cells were observed before and after FMLP application.

Micropipette aspiration of whole cells was performed on spontaneously deforming active cells, and on cells rendered passive without cytoplasmic deformation by application of EDTA or cytochalasin D. Cells which remained inactive after phagocytosis provided a separate group of passive cells.

Intracellular particle displacement

Neutrophil motion was recorded on video from the inverted microscope at an optical magnification of ~2,000. From the video record, position and time of three to four markers were recorded during a spontaneous cytoplasmic deformation. A video cursor (generated by a photometric analyzer, model 204A; Instrumentation for Physiology & Medicine, Inc., San Diego, CA), which is controlled by a joystick, was used to trace the position of the cell contour and position of the intracellular makers from the video screen. The analog data of cursor position was transferred to a computer (PDP-11, Digital Equipment Corp., Marlboro, MA) via an A/D converter. Time was recorded from a digital time display on the video screen, and the position-time data were stored and used to compute the strains and strain rates.

Measurement error

The accuracy of the video measuring system to record the relative positions of markers may be expressed as the percent error in the triad strain from a known displacement field. The resolution of the video cursor in determining the position of a marker is about ± 0.2 μm. This measurement uncertainty may result in a 20% error of strain if neigboring microspheres are 1–2 μm apart. It should be noted that the magnitude of the strains for most active deformations were large compared to the measurement error.

RESULTS

General observations

Neutrophils incubated with latex microspheres exhibit a range of cytoplasmic activities. Some cells remain passive in a spherical state or immobile with ruffled lammelipodia, other exhibit pseudopod formation and oriented migration.

To investigate the strain in different regions of the cell during pseudopod projection and locomotion, we have identified three morphologically distinct regions of the cell during a cycle of deformation. These are illustrated in Fig. 2. The leading edge of motion, where a gelation front is evident, is denoted as region I. Region II consists of the transition zone between the pseudopod, or the broad gelation front for locomoting cells, and the main cell body. This region often contains a constriction ring. The main cell body, posterior to the transition zone, is identified as region III. This region usually contains the uropod and in cells undergoing pseudopod formation is often observed to be rounded. For locomoting cells, region III may be tapered and contain retraction fibers. Cell deformation such as locomotion and pseudopod formation occurs in the form of motile cycles. A motile cycle may be identified by both transient whole cell shape changes and by the intracellular cytoplasmic displacements.

The majority of data to be reported are from cells with 1.0-μm-diam intracellular microspheres. This marker size yielded the longest unconstrained displacement histories in the focal plane. Strain measurements for the 0.6- and 2.0-μm-diam microspheres are given in Table 1 as the average maximum and minimum cytoplasmic stretch

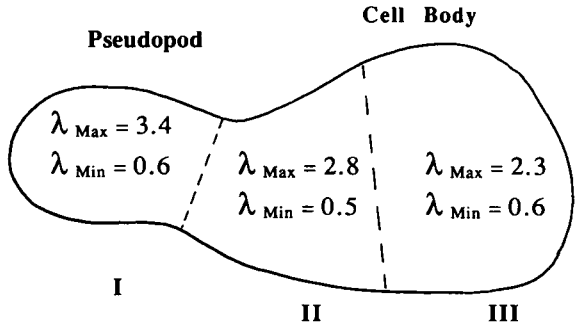

FIGURE 2 A typical contour of a cell with pseudopod. Three regions can be distinguished. Region I with the pseudopod, region II the transition zone to the main cell body, and region III containing the trailing edge or uropod. Average maximum and minimum cytoplasmic stretch ratios for individual motile cycles are shown within each region for measurements with 1-μm microspheres. The average whole cell stretch ratios for the same cell cycles ($n = 37$) were $\lambda_{1cell} = 1.2$ and $\lambda_{2cell} = 0.9$ and represent a smaller deformation than the corresponding cytoplasmic stretch ratios.

TABLE 1 Cytoplasmic stretch ratios in active neutrophils

Region	I		II		III	
λ_{triad}	Max	Min	Max	Min	Max	Min
μm						
0.6	1.8	0.3	2.1	0.4	N/A	N/A
1.0	3.4	0.6	2.8	0.5	2.3	0.6
2.0	3.4	0.3	2.7	0.9	1.9	0.5

Maximum and minimum principal stretch ratios measured from triads of 0.6-, 1.0-, 2.0-μm-diam microspheres in regions I–III are shown.

ratios. The triads with 0.6-μm microspheres revealed larger strains than the 1.0- and 2.0-μm microspheres. However, these smaller microspheres could be observed only for short deformation histories. Like the granules, they rapidly move out of the focal plane. The 2.0-μm markers more readily remained in the focal plane, but are large in comparison to the cytoplasmic organelles within the cell matrix. These markers were often observed to be restricted in their displacements, yielding lower values of triad strain. In fact the 2.0-μm microspheres were not observed to enter the pseudopod region.

Pseudopod projection and locomotion

An example of a single pseudopod projection and retraction is provided in Fig. 3. Video images from the microscope with the digitized cell contours are shown. Initial stretch ratios ($\lambda = 1$) are drawn at the triad's centroid orthogonal to the laboratory reference. Subsequent frames reveal extensions and contractions (depicted as relative changes in the line element length) of the stretch ratios oriented in the Eulerian or spatial principal directions of strain.

Pseudopod formation of this form is accompanied by an

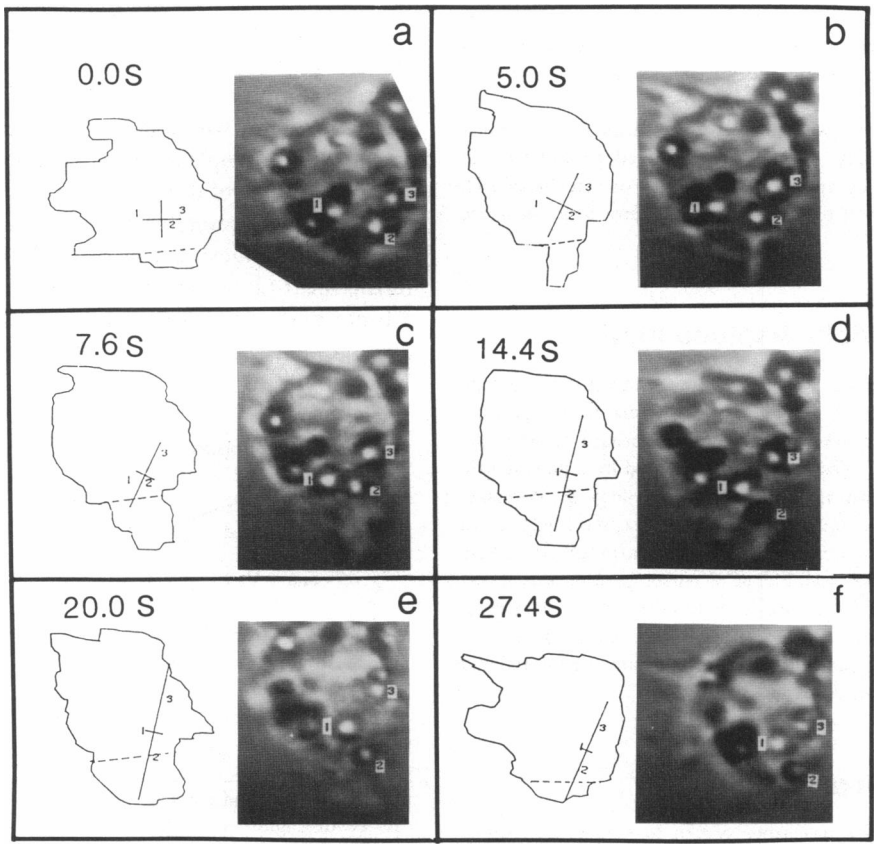

FIGURE 3 Individual record of freely suspended neutrophil during pseudopod projection. The micrographs were taken from the television screen, providing the cell contour and the position of the internalized microspheres. The cell contour and cytoplasmic stretch ratios are shown to the left; the dashed line indicates the transition zone between cell and pseudopod. The three markers which were used to determine cytoplasmic strains are labeled 1, 2, 3 in counterclockwise direction at time zero. The stretch ratios and principal directions are shown in each frame ($\lambda = 1$ at $t = 0$ s) together with the position of the microspheres depicted as numbers 1, 2, and 3. The length scale is such that the cell diameter at $t = 0$ corresponds to ~8 μm.

exclusion of granules. The projected surface area of this region is increased until an elongated morphologically distinct projection has formed at $t = 7.6$ s in region I. The broken line drawn in the cell contours represents a separation between regions I and II. A constriction ring may be identified at the pseudopod base with a characteristic concentric narrowing of the cell as seen at $t = 7.6$ s. The constriction ring travels along the cell body and eventually vanishes in regions II or III. Subsequent to constriction ring formation the pseudopod broadens ($t = 14.4$ s), at which time solation of the cytogel begins. This is marked by the onset of random granule motion in regions I and II. During pseudopod retraction the cell returns to a partially spherical, although still deformed shape ($t = 27.4$ s). Triad strain depicted by the stretch ratio within the cell contours of Fig. 3 reveals a progressive elongation in the direction of pseudopod formation, reaching a maximum toward the end of the cycle ($t = 20.0$ s). At the particular triad position shown in Fig. 3, the strains do not return to their initial values.

Cells may adopt many different shapes during any given pseudopod cycle. The time course of a pseudopod cycle ranges from as short as 12 s to more >1 min with a mean of 31 s ($n = 37$).

A cell undergoing locomotion may be differentiated from one projecting pseudopods by the polarized shape and the broad leading edge, often denoted as a gelation front. Neutrophils may undergo a random, spontaneous cyclic locomotion in the absence of a chemotactic stimulus, as shown in Fig. 4. The locomotion cycle begins with the projection of a broad veil of lamellipodia which may be adherent to the substrate ($t = 0.0$ s). Subsequently, a constriction ring forms just posterior to the leading edge ($t = 23.5$ s). As the construction ring enters region II the projected surface area of region I increases along with both components of cytoplasmic strain ($t = 42.0$ s). Region III may acquire an elongated, tapered, or rounded configuration which is often observed to be adherent to the substrate. As the cell reaches maximum elongation, cytoplasmic streaming from the rear toward the leading edge occurs. This phenomenon coincides with the detachment and retraction of the uropod.

The motile cycle is completed in this case, not when the overall cell shape returns to an initial configuration but when the triad approaches a new configuration and its motion has subsided ($t = 59.2$ s). Cytoplasmic strain for this cycle is depicted by the stretch ratios drawn at the triad's centroid. Elongation of the triad is coupled to cell elongation and its direction by $t = 29.9$ s. At $t = 42.0$ s the plane of the constriction ring passes and strongly deforms the triad, causing a large local shear strain. The cell shape and cytoplasmic strains do not return to the initial state at the end of the cycle.

During locomotion cells usually form broader lammelipodia than during pseudopod projection. Locomoting cells also exhibit stronger adhesion, especially at the leading edge. Constriction rings are evident and cells in locomotion appear to move through these stationary rings with a net forward displacement. A chief difference between locomotion and pseudopod projection is that region I shows less spreading for pseudopod projection. Pseudopods tend to retract back into the cell body, whereas the

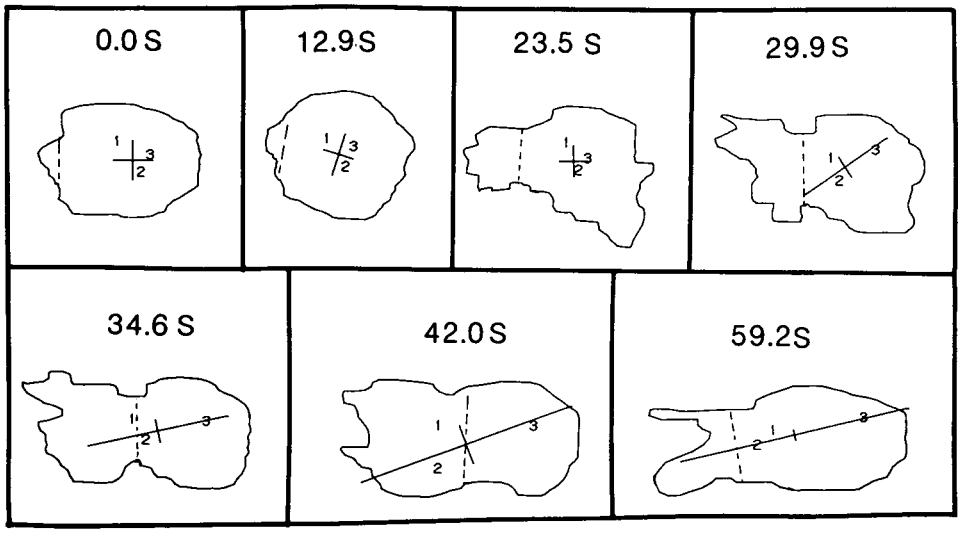

FIGURE 4 Cell contours and cytoplasmic stretch ratios of a neutrophil undergoing locomotion toward the left side. Notation is the same as in Fig. 3. Dashed line indicates the position of the constriction ring passing from the pseudopod over the main cell body during locomotion. Note the large cytoplasmic strain at the point where the constriction ring reaches the microspheres.

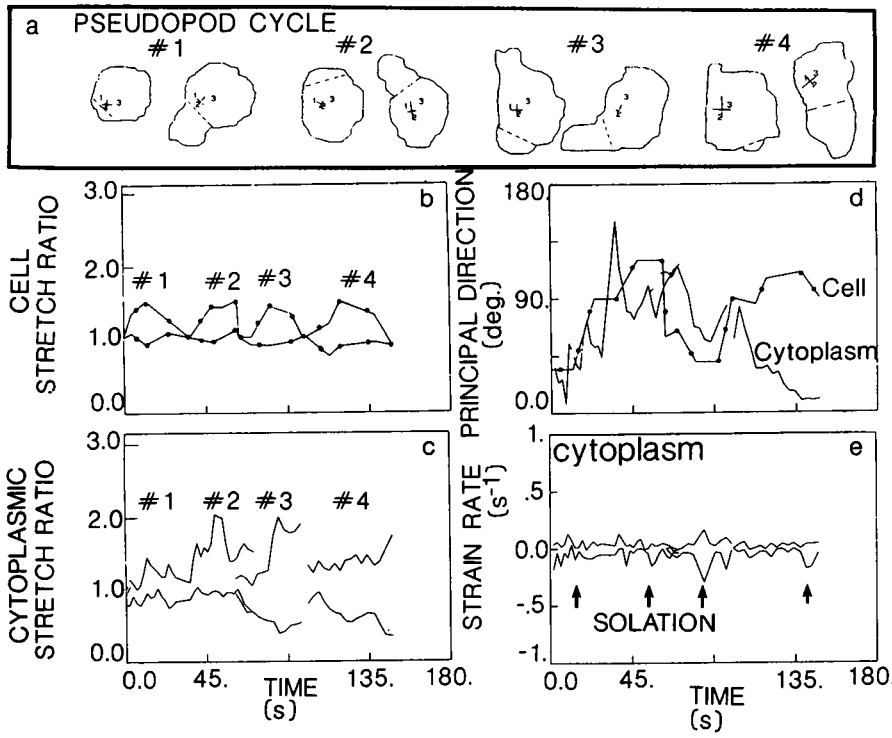

FIGURE 5 A single neutrophil during multiple pseudopod projections. (*a*) Cell contours and cytoplasmic stretch ratio's and principal directions. Dashed lines show the transition zone between pseudopod and main cell body. Times are: 1: 0 and 12 s, 2: 33 and 54 s, 3: 82 and 99 s, 4: 110 and 148 s on the left and right respectively; (*b*) Magnitude of the whole cell stretch ratios, λ_{1cell}, λ_{2cell}. (*c*) Cytoplasmic stretch ratio, (*d*) their principal directions, and (*e*) the cytoplasmic strain rates. The instances of solation at the base of the pseudopod are indicated by the arrows in panel *e*.

cell in locomotion detaches from the uropod and pulls the posteriod portion (region III) forward in the direction of locomotion.

Pseudopod projection over several motile cycles

Fig. 5 shows cell contours (Fig. 5 *a*) from the undeformed and fully extended state of four pseudopod cycles over 148 s of observation. Whole cell stretch ratios (Fig. 5 *b*), cytoplasmic stretch ratios (Fig. 5 *c*), and the time history of the Eulerian principal strain direction (Fig. 5 *d*) are shown together with the direction of maximum cell elongation. The cell is seen to undergo four cyclic elongations which reaches cell stretch ratios of about $\lambda_{cell} = 1.5$ at full pseudopod cell extension, and do not necessarily return to their initial value after pseudopod retraction. The contractile stretch ratio in the perpendicular direction is smaller with about $\lambda_{cell} = 0.85$. The cell stretch history shows that after each pseudopod the cell returns close to its original shape. The rate of pseudopod projection and retraction are similar but not identical.

With the exception of pseudopod cycle No. 1 (Fig. 5), the internal cytoplasmic strains clearly exceed the whole cell stretch ratios both in elongation and shortening (panel *c*). The Eulerian strain principal directions are reasonably well aligned with the exception of pseudopod cycle No. 4 during which the triad is remote (in Region III) from the pseudopod.

The cytoplasmic strain rates (Fig. 5 *e*) reveal relatively constant values during repeated cycles of elongation and shortening. Average values for the principal strain rates reach $D_{MAX} = 0.23 \pm 0.1\ s^{-1}$ and $D_{MIN} = -0.12 \pm 0.06\ s^{-1}$. For each pseudopod cycle, the shear rate reaches maximum and minimum values during the solation phase when the pseudopods are retracting. Both granules and the microsphere markers are subject to rapid random motion during this phase. The principal directions of the rate of deformation were computed from the solution of an eigenvalue problem similar to Eq. 10 for the strain tensor. The angle of the principal directions of strain rate was found to vary by up to 180° during short periods of the order of seconds, and may in part reflect numerical error in the eigenvalue solution. For example in Fig. 5, the strain rate which is sensitive to small fluctuations in the rate of change of intermarker distance over each time step, exhibited changes in the strain rate's principal direction of ~120° within the first 5 s.

Neutrophil chemotaxis after application of FMLP

Neutrophils show several responses to the chemotactic stimulus FMLP, two of the most prominent are cell spreading on the substrate followed by cell polarization. An example of this behavior is illustrated in Fig. 6. Cell contours of Fig. 6 *a* shows a cell spread and adhered to the substrate. The triad is initially located in region II posterior to the gelation front (indicated by the dashed line). A pseudopod is projected to the right in the direction of the micropipette with the chemotactic agent. Cell polarization proceeds at $t = 24.6$ s and the constriction ring passes the triad at about this time. The stretch ratio history (Fig. 6 *b*) describes a reversible deformation history in which the cell and triad return close to the reference state. During cell polarization, the triad undergoes a shear deformation in which the principal direction is oriented with that of the cell (Fig. 6 *c*). Elongation of the triad reaches twice that of the cell, the contractile strains of the cell and triad are closely coupled in time and magnitude. Pseudopod retraction at $t = 35.0$ s initiates the return of the cytoplasmic stretch ratio toward the reference state and is concommitant with solation of the polymerized cytoplasm. The rate of deformation (Fig. 6 *d*) reveals a cyclic movement with small amplitudes, characteristic of the marker motion both in dilation and contraction.

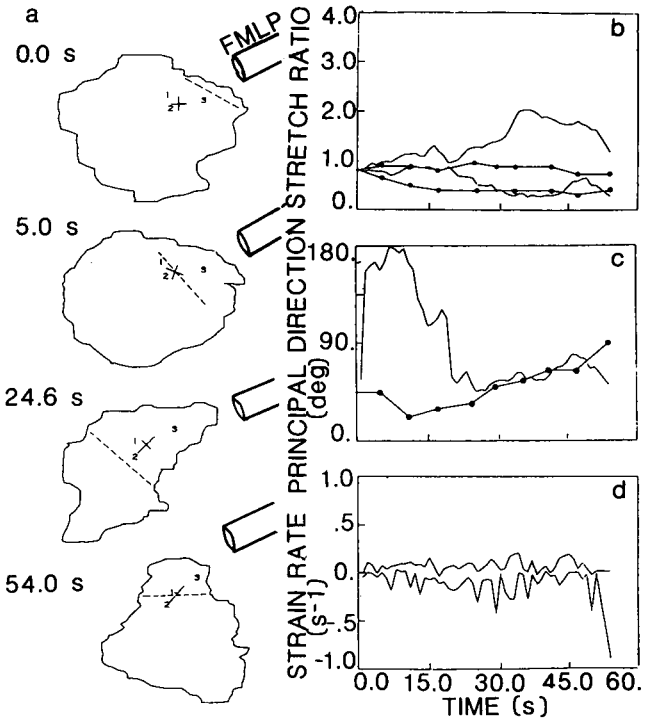

FIGURE 6 Pseudopod projection in a neutrophil due to stimulation with 10^{-7} M FMLP diffusing from a pipette placed adjacent to the cell. Cytoplasmic and whole cell stretch ratios (*b*), their principal directions (*c*), and cytoplasmic strain rates (*d*) are shown by the continuous lines. The lines with points in *b* and *c* show the corresponding quantities for the whole cell at the same instances of time.

Spatial distribution of strain

Fig. 7 shows two separate triads in a cell during pseudopod projection. Triad No. 1 is initially located in region II, and triad No. 2 in region III in this case. The strain history for traid No. 1 is closely correlated with the onset of pseudopod formation (Fig. 7 *b*). This triad is subject to two successive shear deformations, one at $t = 5.0$ s, followed by the second larger shear at $t = 30.0$ s. As the constriction ring plane ($t = 14$ s, Fig. 7 *a*) reaches that of traid No. 1, large deformation ensues. The Eulerian strain principal directions for the cell and triad No. 1 follow

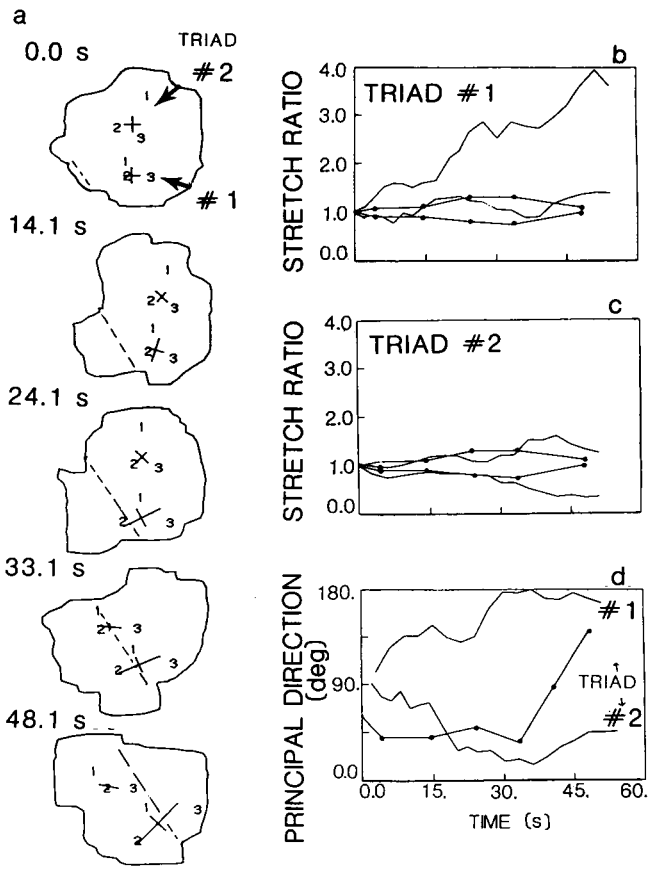

FIGURE 7 Cytoplasmic strains measured via two different triads in the same neutrophil at the same time during spontaneous pseudopod projection. The dashed line in the cell contours of *a* shows the position of a constriction ring formed by the cell. The line with points in *b–d* show the corresponding quantities for the whole cell at the same time instances.

similar time histories but are misaligned by ~30° (Fig. 7 *d*). Traid No. 2 is subject to only a moderate extension in response to the initial cell shape change. A large shear in triad No. 2 at $t = 35.0$ s occurs when the plane of the constriction ring passes (Fig. 7 *c*). Solation and pseudopod broadening proceed after the constriction ring reaches region III and effects a large elongation for each of the two traids. Only triad No. 2 reacts to a second localized pseudopod, depicted in the upper left of the final contour, causing further triad contraction and elongation. The principal direction of triad No. 1's deformation is not oriented in the cell's major axis of deformation (Fig. 7 *d*).

Average regional strains

A consistent observation is the large cytoplasmic strains as compared with the relatively modest cell shape change. This is summarized in Fig. 2 in which the mean triad stretch ratios for peak elongation and lateral contraction are provided within each region. The cytoplasm experienced on average threefold greater elongations and twofold larger contractions than did the cell contour during a motile cycle. The strain distribution for the 1.0-μm microspheres in region I revealed moderate elongation and large contraction. Region II revealed an almost symmetric distribution of strains in contraction and elongation. Cytoplasmic strains in region III show large elongations and moderate contractions.

In many cases the principal direction of Eulerian triad strain correlated closely with the major axis of cell deformation. A weak correlation was found between triad and cell extension in region I compared to that in region II. Virtually no correlation between cell shape change and triad strain direction was found in region III.

Active vs. passive cytoplasmic strain

A comparison between simultaneous cell and cytoplasmic stretch ratios during spontaneous active motility is shown in Fig. 8 *a*. The stretch ratios are derived from 37 cells in regions I–III over a single motile cycle. In this way the maximum elongation of the cell may be correlated with the corresponding maximum cytoplasmic stretch ratio, and separately the cell lateral contraction with the minimum cytoplasmic stetch ratio. The small slope of the correlation line ($m = 0.09$) shows the large intracellular strains for only modest whole cell deformations. This may be compared with intracellular strains in the so-called passive state which are deformed only by an externally applied stress. Cells were treated either with EDTA (1 g%) to deplete extracellular calcium, or cytochalasin-D (0.5 μg/ml) to prevent F-actin formation. Both suppress pseudopod formation and locomotion. A micropipette was used to achieve whole cell aspiration or to deform just the region of the cell where the triad was located. The triad and cell strain were then measured using the same procedure as for active cells. Cytochalasin-treated cells achieved large deformations during aspiration, whereas the cytoplasm of EDTA-treated cells at the same aspiration pressure exhibited small deformation into the pipette reflecting considerably stiffer properties. Yet comparison of the maximum and minimum stretch ratios for the cell and cytoplasm reveals a relatively close correlation, with a slope close to one (Fig. 8 *b*). Thus, applied cell deformation produced a proportional elongation and contraction of the cytoplasm over a wide range of cell strains. Untreated cells which remained spontaneously inactive also yielded a close correlation between whole cell and cytoplasmic strain during cell aspiration.

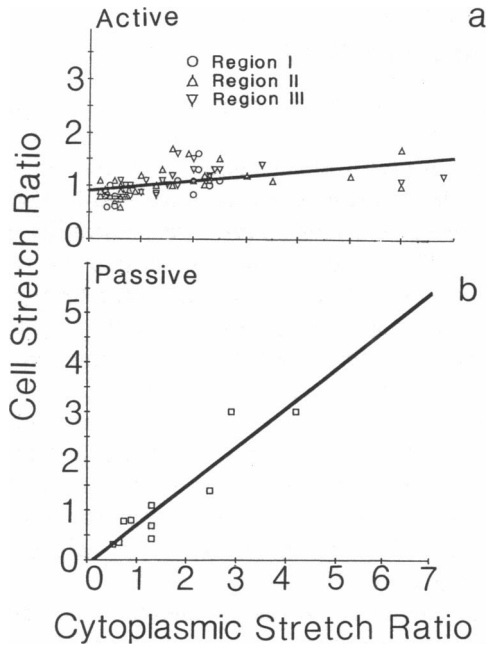

FIGURE 8 The whole cell stretch ratios of neutrophils as a function of cytoplasmic stretch ratios (*a*) during spontaneous active motility ($n = 37$ cells) and (*b*) in passive neutrophils without pseudopod formation ($n = 5$ cells). In case *b* the cells were treated with EDTA or cytochalasin B and deformed by whole cell aspiration into a micropipette while cytoplasmic strains were measured. The line in *b* has a slope of $m = 0.78$, whereas in (*a*) the slope is only $m = 0.09$.

Homogeneity of cytoplasmic deformation

An example in which four markers were used to form two triads, one within the other, provides a method of scaling the homogeneity of deformation (Fig. 9). Triad No. 1 and triad No. 2 are located inside the gelation front region I

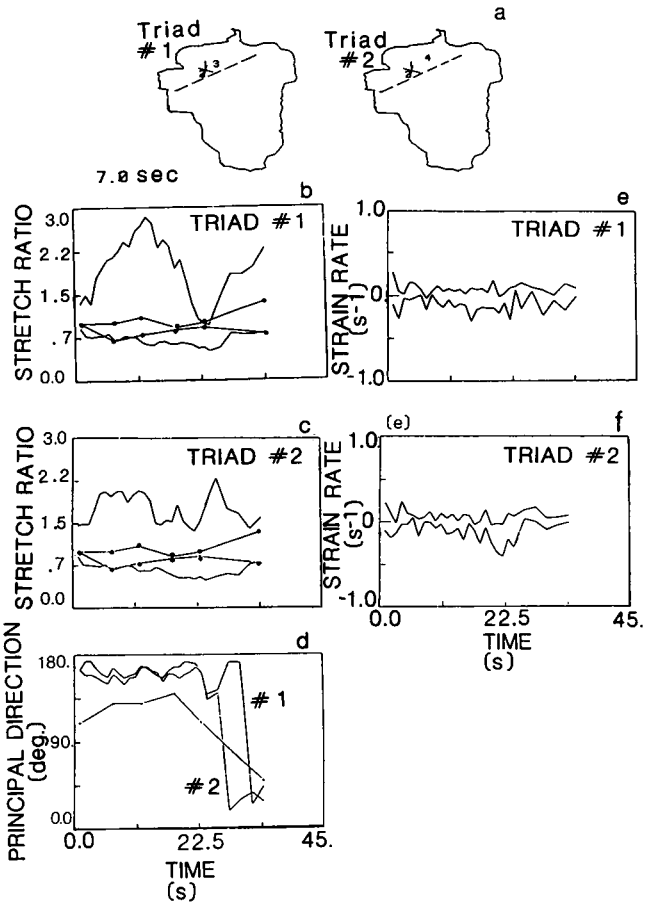

FIGURE 9 Two triads are formed from four markers. Triad 1 contains markers No. 1, 2, 3; triad 2 contains markers No. 1, 2, 4. Cytoplasmic strains were measured simultaneously during two successive pseudopod projections. Cell contours (*a*) are shown just after the first pseudopod is projected to the left-hand side. Stretch ratio histories for the cell (line with solid dots) and cytoplasm are shown for triad 1 (*b*) and triad 2 (*c*). Eulerian principal directions (*d*) for both triads and the cell contour. Strain rates for triad 1 (*e*) and triad 2 (*f*) are shown.

during the deformation history as shown in the cell contours of Fig. 9 *a*. A small broad pseudopod forms to the left of the two triads at $t = 7$ s. Triad No. 1 undergoes an elongation and lateral contraction which is synchronized and in the direction of pseudopod formation (Fig. 9 *b*). Triad No. 2 exhibits a time course of cytoplasmic contraction similar to that of triad No. 1, but with an elongation which is 25% smaller (Fig. 9 *c*). The principal directions of Eulerian strain are similar for the two triads (Fig. 9 *d*).

A second pseudopod is projected at $t = 23$ s in the direction of about one o'clock, just above marker No. 4. An elongation is registered in triad No. 2 which precedes by ~3 s that experienced by triad No. 1, and was synchronized with the cell's elongation (Fig. 9 *b*). A comparison of the deformation histories for the two triads reveal strains which are closely correlated with respect to time and direction. The differences in the magnitude of elongation are a function of the location of each respective triad relative to the site of pseudopod projection and to a lesser extent the initial spacing of the triad.

The rate of deformation (Fig. 9, *e* and *f*) shows the two triads to have closely synchronized strain rates which become slightly uncoupled during the second pseudopod projection, where triad No. 2 experiences a slightly larger rate of elongation.

DISCUSSION

The main features which may be derived from the current strain analysis are as follows: (*a*) Large cytoplasmic strains are measured in cells exhibiting at the same time relatively modest shape changes. (*b*) The direction of overall cell deformation and the principal direction of cytoplasmic strain frequently coincide. (*c*) Cytoplasmic strains vary with cell region and over the time course of a motile cycle. (*d*) Morphologic features such as constriction rings, local adherence, and cell polarization were associated with specific cytoplasmic strains.

The process of active force generation which enables the cell matrix to achieve large strains, as well as fine coordination of localized strains (i.e., lammelipodia, organelle motion), makes the cytoplasm unique. It behaves fundamentally different from passive materials, biological or otherwise, which exhibit strains in response to an external applied stress field. In active deformation, a stress and large strain field are achieved within the cytoplasm through a high-energy, phosphate-mediated chemicomechanical transformation.

Cytoplasmic strain compatability and homogeneity

In some cases, the observed triad displacement fields may not be compatible in the usual continuum sense (Fung, 1969). Physically, compatibility requires that a body which is initially divided into small elements and then subjected to deformation, retains any two neighboring elements as neighbors. The strain data herein represents the deformation within localized cytoplasmic areas on the order of 1 μm^2, where the marker displacements appeared to be compatible throughout the region.

Cytoplasmic stretch ratios measured simultaneously in different regions of the same cell, as shown in Fig. 7, yield strains which may differ in magnitude and time course. This indicates that the strain field is nonuniform, at least over the cell body. A more localized cytoplasmic strain

measurement using two overlapping triads which mapped the strain within a complex deformation history (Fig. 9), yielded strains which were closer in amplitude and direction. A higher resolution analysis of cytoplasmic strain homogeneity would require a comparison of simultaneously measured strains of progressively smaller areas, with yet smaller cytoplasmic markers. It is apparent that actively deforming cytoplasm is a complex material and exhibits nonhomogeneity even on a length scale of ~ 1 μm (e.g., Fig. 9), where we are measuring the average properties and interaction of thousands of molecules.

Regional strain variation

A comparison of the dominant strain fields in each of the three regions showed I to be mostly contractile with small elongations. Markers in region I also registered the smallest displacements in comparison to markers in Region III with the longest marker excursions. The strain histories of region I revealed a deformation which more frequently returned towards the reference configuration than those of regions II and III. Region I has been shown to contain a high concentration of F-actin (Valerius et al., 1981; Sullivan and Mandell, 1983) and can exhibit properties resembling those of an elastic material (Schmid-Schönbein et al., 1982).

Region II is the site were the largest shear strains are recorded along with the most complex displacement fields; for example, motion of a marker through the plane of two other markers, thereby inverting the original triad. Deformation histories in region II were largely irreversible, yielding finite cytoplasmic strains with respect to the reference configuration.

Region III was characterized by large extensional strains in which markers were displaced toward the leading edge of motion or pseudopod tip, and in the process revealed nonhomogeneous displacement fields in some cases. At the completion of the motile cycle in region III the final triad configuration seldom returned toward the initial reference configuration, resulting in large irreversible strain histories.

Mechanisms of cytoplasmic deformation

Several of the cytoplasmic displacement fields observed may be the result of slipping of cytoplasmic layers past one another. A sliding mechanism in which a dislocation exists between two neighboring cytoplasmic layers in effect may result in an incompatible displacement field. Contraction of the actin network, as occurs during the polymerization process, may cause a small decrease in local hydrostatic pressure but is probably not sufficient to effect the large net displacement of cytoplasm which we observed. One mechanism which may serve to derive protopod extension is the polymerization of monomeric actin. This so-called "polymerization strain" is thought to occur at the pseudopod (Schmid-Schönbein and Skalak, 1984; Zhu and Skalak, 1988). The process has been modeled as a two-step process with isotropic volumetric contraction due to exclusion of granules accompanied by a shear strain due to alignment of actin fibers. Supporting such a model are observations of small uniform contractions of cytoplasm observed in region I close to the leading edge. The majority of deformations made posterior to the protopod were characterized as shear strains. Active sliding of actin bundles may be achieved through the action of myosin oligomers by a cross-bridge mechanism similar to sarcomeres in skeletal muscle (Huxley, 1969; Stossel and Yin, 1982; Sheetz and Spudich, 1983). This mechanism could effect the large extensions recorded in regions II and III.

The constriction ring, frequently observed in region II, coincides with the occurrence of large internal shear strains. Constriction rings travel like peristaltic waves along the cell body after surrounding concentrically the unfolded cell nucleus (Schmid-Schönbein et al., 1982). They may function to coordinate the conduction of the motive force from region I, posteriorly along the cell body. Oster et al. (1984) implicated this event as the initiator of the force generation process. Pathline analysis of marker motion in regions II and III show that large displacements occur close to the center of the cell as opposed to the periphery or cortical region proximal to the plasma membrane (Simon, 1988). These observations are not necessarily consistent with the concept of a contractile cortical layer within the submembrane cortex as postulated for passive cells, (Evans et al., 1984; Dong et al., 1988) because internal strains exceed strains in the membrane.

The relatively large contractile strains in region II appear to be temporally and spatially coupled to the passage of the constriction ring. The large extensional strains along the cell's longitudinal axis show that the cytoplasm maintains its mobility and suggests the existence of a transition zone at the plasma membrane.

Microspheres as cytoplasmic markers

Micropipette studies suggest that the whole cell deforms as an incompressible medium (Schmid-Schönbein et al., 1981). For local regions of the cell cytoplasm where free water movement between the actin matrix may occur, the assumption of local incompressibility of the cell cytoplasm may not be made a priori. Incompressibility of the cytoplasm requires that the product of the stretch ratios equal to one ($\lambda_1\lambda_2\lambda_3 = 1$). In the current experiments

strain was measured in the focal plane and the product $\lambda_1\lambda_2$ assume values above and below 1. In the extreme case $\lambda_1\lambda_2$ reached values as large as six (Fig. 4). Because λ_3 was not measured, the question of local cytoplasmic incompressibility at this point remains unresolved.

There is a possibility that the phagocytosed microspheres subject the neutrophil to conditions which alter its motile characteristics and therefore the cytoplasmic strain. These experiments were performed with cells which had low numbers of internalized microspheres. A local increase in sphere density had minimal effect on the measured strains. An alternative would be to measure the motion of organelles such as the granules. However, these too impose their affect on the deformation of the cytoplasm surrounding them and they may be subject to specialized interactions with the cytoplasm. Furthermore, these granules are difficult to use as markers because they travel in and out of the focal plane at a rapid rate. We have attempted to estimate the effects of various size markers (Simon, 1988). The results indicate that marker size between 0.6 and 2.0 μm do not greatly affect the magnitude of the cytoplasmic strain measurements (Table 1).

Cytoplasmic forces

The cytoplasmic displacement of active neutrophils may be the result of several physical forces involved. A stress may be transmitted via preformed actin microfilaments or microtubules from one part of the cell to another. The associated displacement is denoted as u_i^σ. Actin polymerization or the active interaction between myosin and associated proteins provide a displacement u_i^P, which may be limited to those cytoplasmic regions where these reactions take place. Finally, there is the thermal Brownian motion with associated random displacement u_i^B. In active cells this displacement is negligibly small with the exception of a short-lasting local solation region at the base of the pseudopod during retraction. The small value of u_i^B is largely due to the high cytoplasmic stiffness of neutrophils (Schmid-Schönbein et al., 1982) and can be reversed by cytochalasin B treatment of the cell which prevents actin cross-linking and converts the cytoplasm to a more fluid state (Simon, 1988). The resultant net microsphere displacement u_i is then:

$$u_i = u_i^\sigma + u_i^B + u_i^P. \tag{20}$$

The Eulerian or Lagrangian strains computed from this displacement field cannot be separated into individual components due to the nonlinearity of the displacement gradient-strain relationships (Eq. 6, *a* and *b*).

Cytoplasmic stress

Because most cells in the current measurements are either in free suspension or have only limited points of attachment, the external applied stresses are approximately zero. But internal stresses in the molecules of the cell matrix may exist. This includes a residual stress in resting cells as well as nonuniform stresses due to actin polymerization and macromolecular interaction. The behavior of cells after cytochalasin treatment showed a large increase of granule or marker Brownian motion, indicating that passive cross-linked cytoplasm may not be stress free. Polymerization or depolymerization can effect nonuniform stress fields resulting in active motion (Zhu et al., 1989; Zhu and Skalak, 1988). The cycoplasmic stress may be limited to the cytoskeleton if water in the aqueous phase is free to move between the macromolecules.

Future developments

The current technique can be applied to analysis of many different cell mechanics problems. It should be extended to three-dimensional strain measurements by tracking four markers in different planes. The analysis may be applied to other markers, such as fluorescent labels and injected microspheres detectable in living cells.

The authors wish to thank Professor R. Skalak for valuable comments.

This research was supported by United States Public Health Service grant HL-10881.

Received for publication 28 July 1989 and in final form 22 March 1990.

REFERENCES

Allen, R. D. 1981. Motility. *J. Cell Biol.* 3:1485–1555.

Berlin, R. D., and S. M. Oliver. 1978. Analagous ultrastructure and surface properties during capping and phagocytosis in leukocytes. *J. Cell Biol.* 77:789–804.

Davis, B. H., R. J. Walker, and C. B. Pearson. 1982. Membrane activity and topography of f-met-leu-phe treated polymorphonuclear leukocytes: acute and sustained responses to chemotactic peptides. *Am. J. Pathol.* 108:206–219.

Dong, C., R. Skalak, K. L. P. Sung, G. W. Schmid-Schönbein, and S. Chien. 1988. Passive deformation analysis of human leukocytes. *J. Biomech. Eng.* 110:27–35.

Evans, E., and B. Kukan. 1984. Passive mechanical behavior of granulocytes based on large deformation and recovery after deformation tests. *Blood.* 64:1028–1035.

Fujiwara, K., and T. D. Pollard. 1976. Fluorescent antibody localization of myosin in the cytoplasm, cleavage furrow, and mitotic spindle of human cells. *J. Cell Biol.* 71:847–875.

Fung, Y. C. 1969. *A First Course in Continuum Mechanics.* Prentice-Hall Inc., Englewood Cliffs, NJ.

Huxley, H. E. 1969. The mechanism of muscular contraction. *Science (Wash. DC)*. 164:1356–1366.

Malech, H. L., R. K. Root, and J. I. Gallin. 1977. Structural analysis of human neutrophil migration: centriole, microtubule, and microfilament orientation and function during chemotaxis. *J. Cell Biol.* 75:666–693.

Oster, G. F., and G. M. Odell. 1984. The mechanochemistry of cytogels. *Physica*. 12D:333–350.

Schliwa, M. 1986. The Cytoskeleton: An Introductory Survey. Springer-Verlag, Berlin.

Schmid-Schönbein, G. W., and R. Skalak. 1984. Continuum mechanical model of leukocytes during protopod formation. *J. Biomech. Eng.* 106:10–18.

Schmid-Schönbein, G. W., R. Skalak, K.-L. P. Sung, and S. Chien. 1982. Human leukocytes in the active state. *In* White blood Cells, Morphology and Rheology as Related to Function. U. Bagge, G. V. R. Born, and P. Gaehtgens, editor. Martinus Nijhoff, The Hague. 21–31.

Schmid-Schönbein, G. W., K.-L. P. Sung, H. Tözeren, S. Chien, and R. Skalak. 1981. Passive mechanical properties of human leukocytes. *Biophys. J.* 36:248–256.

Senda, N., N. Shibata, N. Tatsumi, K. Kondo, and K. Humada. 1969. A contractile protein from leukocytes: its extraction and some of its properties. *Biochim. Biophys. Acta*. 181:191–200.

Sheetz, M. P., and J. A. Spudich. 1983. Movement of myosin-coated fluorescent beads on actin cables in vitro. *Nature (Lond.)*. 303:30–35.

Shields, J. M., and W. S. Haston. 1985. Behaviour of neutrophil leukocytes in uniform concentrations of chemotactic factors: contraction waves, cell polarity and persistance. *J. Cell Sci.* 74:75–93.

Simon, S. I. 1988. Biophysical analysis of neutrophil motility. Ph.D. thesis. University of California, San Diego.

Simon, S. I., and G. W. Schmid-Schönbein. 1988. Biophysical aspects of microsphere engulfment. *Biophys. J.* 53:163–173.

Stossel, T. P., and J. H. Hartwig. 1976. Interactions of actin, myosin and a new actin-binding protein of rabbit pulmonary macrophages H. Role in cytoplasmic movement and phagocytosis. *J. Cell Biol.* 83:602–619.

Stossel, T. P., and H. L. Yin. 1982. The Mechanism of Phagocytosis: Phagocytosis Past and Future. Academic Press, Inc., New York.

Sullivan, J. A., and G. L. Mandell. 1983. Mobility of human polymorphonuclear neutrophils: microscopic analysis of substrate adhesion and distribution of F-actin. *Cell Motil.* 3:31–46.

Taylor, D. L., and J. S. Condeelis. 1979. Cytoplasmic structure and contractility in amoeboid cells. *Int. Rev. Cyt.* 56:57–144.

Valerius, N. H., O. Stendohl, J. H. Hertwig, and T. P. Stossel. 1981. Distribution of actin-binding protein and myosin in polymorphonuclear leukocytes during locomotion and phagocytosis. *Cell.* 24:195–202.

Zigmond, S. H. 1978. Chemotaxis by polymorphonuclear leukocytes. *J. Cell Biol.* 77:269–287.

Zhu, C., and R. Skalak. 1988. A continuum model of protrusion of pseudopod in leukocytes. *Biophys. J.* 54:1115–1137.

Zhu, C., R. Skalak, and G. W. Schmid-Schönbein. 1989. One-dimensional steady continuum model of retraction of pseudopod in leukocytes. *J. Biomech. Eng.* 111:69–77.